Part III Systems Biology Project Report

Modelling Mitochondrial Liver Toxicity With Oxygen and Cell Density Gradients

Xingze Xu, University of Cambridge

Supervisor: Dr Giovanni Di Veroli, AstraZeneca plc.

Deputy supervisor: Dr Aydar Uatay, AstraZeneca plc.

Number of words: 4974

Declaration

Name: Xingze Xu

College: Homerton

Project title: Modelling Mitochondrial Liver Toxicity With Oxygen and Cell Density Gradients

I understand the University's definition of plagiarism. I declare that, in accordance with Discipline regulation 6, this dissertation is entirely my own work except where otherwise stated, either in the form of citation of published work, or acknowledgement of the source of any unpublished material.

Signature: *Xingze Xu*   Date: 27/04/2022

Summary

Drug-induced liver injury (DILI) has become a major safety concern in drug development, and various models of DILI have been developed for pre-clinical screening. This thesis presents Systems Model of Drug-Induced Liver Injury (SysDILI), an *in silico* model of human mitochondrial DILI using the holistic approach of systems biology. SysDILI was designed to predict liver toxicity based on mechanism and dose-response of drug while preserving mechanistic and spatiotemporal information for further analysis.

SysDILI consists of four submodels based on partial or ordinary differential equations, describing dynamics of oxygen, mitochondria, cell density of hepatocytes and drug. The submodels were developed and tested independently before being assembled to study and model their interactions. Instead of artificial liver zonation, continuous spatiotemporal distributions were used throughout.

While some of the methods and models in SysDILI build on previous research, original advances have also been incorporated in the design of SysDILI. Oxygen transport by haemoglobin was modelled dynamically using a rebalancing process. Coefficients of drug effects were determined by optimisation to handle the complexity of model. Two Hill equation terms were used to capture the combined effects of energy-dependent apoptosis and necrosis.

After discretisation and numerical simulation of the system in MATLAB, SysDILI successfully predicted the liver toxicity of several known drugs, and the simulated oxygen and cell density gradients also agreed with known results. Further research will aim to add toxicity mechanisms, model longer term DILI and adapt SysDILI to facilitate the *in vitro* model of liver-on-a-chip for practical purpose.

Contents

List of Abbreviations

Abbreviations	Full meanings
DILI	Drug-Induced Liver Injury
MPS	Microphysiological System
ATP	Adenosine Triphosphate
OCR	Oxygen Consumption Rate
ETC	Electron Transport Chain
MMP	Mitochondrial Membrane Potential
SysDILI	Systems Model of Drug-Induced Liver Injury
ROS	Reactive Oxygen Species
Km	Michaelis Constant
LDH	Lactate Dehydrogenase
ALT	Alanine Transaminase
FAST	Fourier Amplitude Sensitivity Testing

1 Introduction

1.1 Drug-Induced Liver Injury

The liver - largest internal organ in the human body, is responsible for a variety of functions, such as production of bile, metabolism of glucose and detoxification. It plays a vital role in metabolism of xenobiotics and hence is vulnerable to drug-induced injury [14]. Drug-induced liver injury (DILI) can occur via many mechanisms, the most prominent ones being mitochondrial dysfunction, bile acid-induced apoptosis and oxidative stress by reactive oxygen species (ROS) or reactive nitrogen species [17].

DILI tends to be non-uniformly spatially distributed across the liver. For example, overdoses of acetaminophen have been reportedto damage the region surrounding the central vein [2]. Such distribution can be explained by the non-homogeneous stucture of the liver: the most basic functional unit, liver acinus, is characterized by zonation [29]. It is commonly accepted that each acinus is divided into three zones from portal triad to central vein, periportal (zone 1), intermediate (zone 2) and perivenous (zone 3), as shown in Figure 1 [22, 11]. Liver zonation is effected in two interacting aspects: (1) gradients of substances, including oxygen, nutrients, xenobiotics, morphogens, hormones and enzymes; (2) gradients of rates in metabolic and regulatory pathways, such as bile acid production and detoxification mostly happening in zone 3 [22]. Therefore, liver zonation plays a crucial role in the study of DILI.

DILI has become a major safety concern in drug development, causing 22 percent of clinical trial terminations and 32 percent of market withdrawals [46]. Even when signs of abnormalities in liver are reported during clinical trials, the regulators might demand additional clinical trials to assess liver safety, which can substantially increase costs of drug development programs.

1.2 Previous Work on Modelling DILI

Due to its importance in drug development, various models of DILI have been developed for pre-clinical screening.
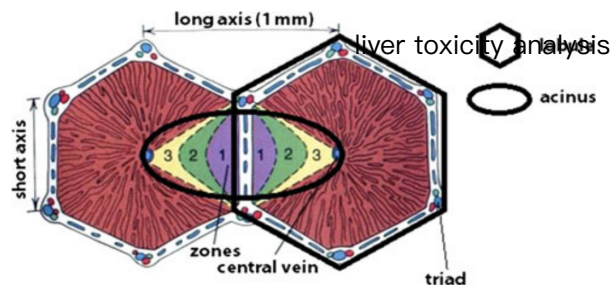
Figure 1 Structure of liver acinus and distribution of the three zones. Diagram from Godoy et al. [11]

.

1.2.1 *In Vitro* Model

Apart from animal models, recent years have seen rapid development of more sophisticated 3D *in vitro* cell culture models, including spheroid, organoid, scaffold, organ-on-a-chip and 3D bioprinting [7].

The spheroid culture system has been commonly used to investigate hepatotoxicity [24]. As opposed to the traditional 2D monolayer cell culture, spheroid culture provides a simple solution to capture spatial gradients of oxygen, drug, nutrients or signalling molecules, because cells in central and peripheral parts of the spheroid have different exposure to the culture medium [7].

Organ-on-a-chip, or microphysiological system (MPS) is another common but more advanced 3D *in vitro* culture model. It utilizes microfluidic devices with specific design and electronic control to simulate the microenvironment and important physiological features of organs. MPS for liver has been relatively well developed, and it is widely used in the pharmaceutical industry for pre-clinical screening. Figure 2 shows a typical design of the device [35]. While it has advantages, MPS also has some limitations – it is complicated and time-consuming, taking up to 7 days to set up before drug intake [35]. Despite efforts to increase the throughput, it remains challenging to detect and interpret the trial results of liver MPS.
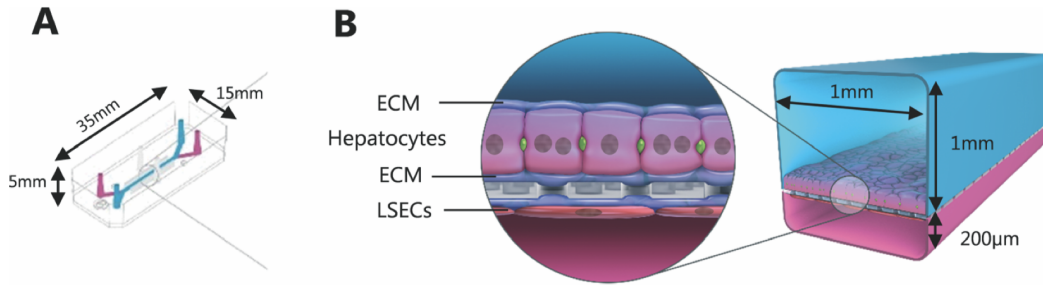
Figure 2 Deisgn of a liver MPS. (A) Dimensions of the MPS; (B) two cell types in the MPS: hepatocypte and liver sinusoidal endothelial cell (LSEC). The interface is coated with extracellular matrix (ECM). Culture media are flown across the cell layers. Diagram from Peel et al. [35]

.

1.2.2 *In Silico* Model

With the operational complexity of *in vitro* models in mind, researchers have developed *in silico* liver models to simulate *in vitro* liver models. Multiphysics simlution software such as COMSOL has been used to investigate the drug distribution in spheroid culture and guide the design of oxygen suppply of liver MPS [25, 23].

There are also more complicated *in silico* models aiming to directly model DILI in human. DILIsym® by Simulations Plus Inc. is a Quantitative Systems Toxicology software for human DILI that consists of a dozen interacting sub-modules, as shown in Figure 3 [1]. As opposed to the multiphyics simulations based on partial differential equations (PDE), DILIsym® is partitioned into the three liver zones each with its set of ordinary differential equations (ODE).

1.3 Systems Model of Drug-Induced Liver Injury (SysDILI)

Systems Model of Drug-Induced Liver Injury (SysDILI) is the *in Silico* DILI model presented in this thesis. Important features of SysDILI are summarised below.

- **Modular**: as in Figure 4, SysDILI consists of four interacting submodels, in the same spirit as the aforementioned DILIsym®. Each submodel was developed and tested independently, so they can be freely assembled. It is also convenient to
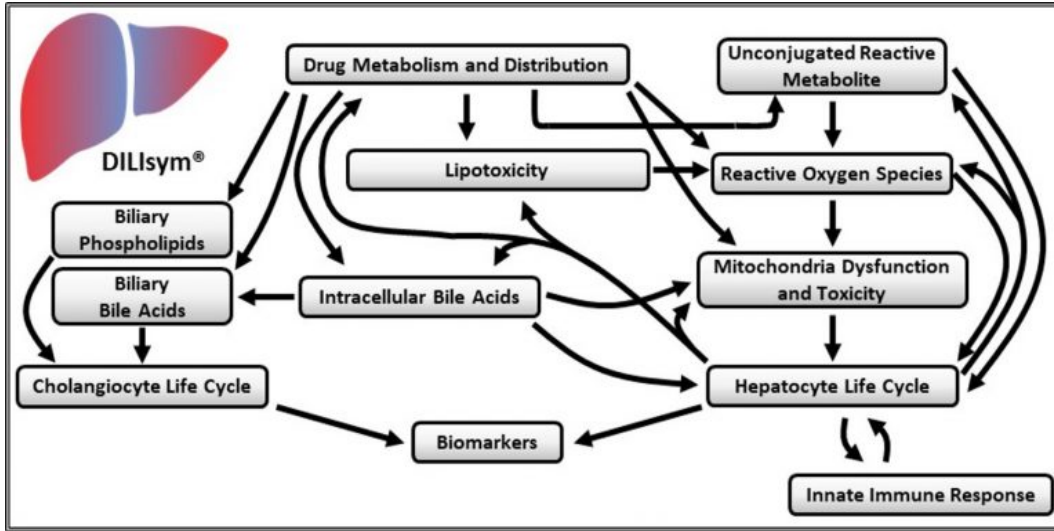
3

Figure 3 Schematic diagram of DILIsym®. The boxes represent submodels that can be inspected alone. An arrow indicates that variables in one submodel affect the rate of one or more processes in another submodel. For example, high concentration of ROS activates apoptosis in hepatocyte life cycle [8]. Diagram from DILIsym® website [1]

.

add new submodels such as glycolysis model without changing the existing ones.

- **Continuous Spatiotemporal Gradients**: the gradients in each submodel are spatially continuous with no artificial zonation, in the same spirit as the aforementioned multiphysics simulations. Also, the temporal dynamics for each gradient was modelled, not just the equilibrium states.

- **Continuum of Domains**: no individual hepatocyte or blood cell in SysDILI. Each domain was modelled as continuum.

- **Mitochondrial Toxicity**: out of the various DILI mechanisms mentioned above, SysDILI currently focuses on mitochondrial toxicity (reasons outlined in Discussion section).

- **Dry Lab**: no experiments have been conducted so far. SysDILI was constructed entirely from published data.

- **Flexible and Customisable**: SysDILI currently models a sinusoid functional unit of human liver, but it can be readily adapted to MPS by changing the shapes

of domains and the boundary conditions, because all the model parameters have been estimated and no gradient data was enforced during model construction.

- **Aim to Be Mechanistic**: the entire process was modelled whenever possible, including the changes in intermediate variables and temporal dynamics. Black box models were only used when mechanistic modelling requires extensive amount of insights or experimental data.
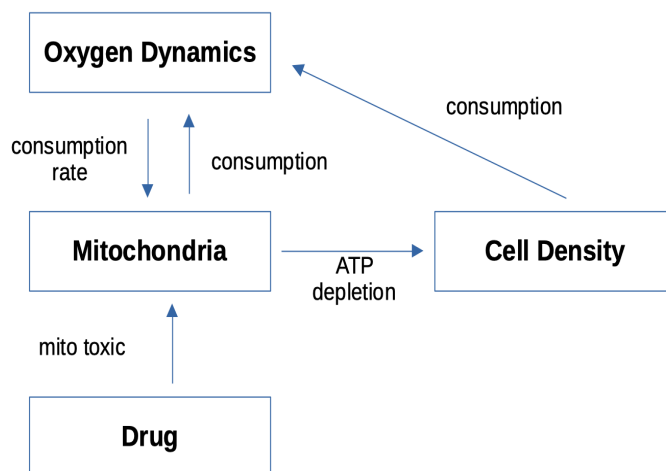

Figure 4 Schematic diagram of SysDILI. The diagram shows the submodels of SysDILI and their interactions. Drug affects mitochondria by its toxicity, which causes ATP depletion and cell death. Oxygen consumed by mitochondria is proportional to cell density, and oxygen concentration conversely affects the state of mitochondrial activities.

The SysDILI model aims primarily to predict DILI based on mechanism and dose-response curve of an unknown drug. In addition to assessing hepatotoxicity, SysDILI was also designed to preserve as much mechanistic and spatiotemporal information as possible. The extra information can be compared against physiological data for validation and might even reveal extra insights. With the flexibility mentioned above, SysDILI can be used to guide the design of MPS and interpret the results.

2 Results

2.1 SysDILI Model

As said in Introduction section, SysDILI consists of four submodels, describing dynamics of oxygen, mitochondria, cell density of hepatocytes and drug, as in Figure 4. These four submodels were selected because they play crucial roles in mitochondrial DILI and interact with each other. Drug inhibits mitochondrial function, which causes ATP depletion and eventually cell death. Mitochondria consumes oxygen in proportional to cell density, while oxygen concentration conversely affects the state of mitochondrial respiration.

2.1.1 Oxygen Submodel

The domain setup of SysDILI is defined in the Oxygen Submodel. In this thesis, a sinusoid functional unit of human liver was modelled, with a hepatic sinusoid extending from portal triad to central vein, surrounded by one layer of hepatocytes.

Since liver sinusoid is a special type of capillary, a design similar to Krogh model of oxygen transport in capillary was used, as shown in Figure 5 [12]. 3D cylindrical coordinate with rotational symmetry about the axial direction was used, and the schematic diagram shows radial and axial directions. There are three domains: sinusoid, hepatocytes and their interface. Oxygen supplied from blood flowing through the left end of sinusoid falls into two categories, plasma oxygen and haemoglobin oxygen. After plasma oxygen diffuses across the interface, it gets consumed by hepatocytes.

2.1.1.1 Model Structure

The submodel is defined by the 5 PDEs listed below.

- **Plasma Oxygen**: convection-diffusion equation was used, because oxygen dissolved in plasma diffuses while being carried by flood flow.

$$\frac{\partial P}{\partial t} = D_1 * \nabla^2 P - \boldsymbol{v} \cdot \nabla P = D_1 * (\frac{\partial^2 P}{\partial r^2} + \frac{\partial^2 P}{\partial z^2} + \frac{1}{r} * \frac{\partial P}{\partial r}) - v * \frac{\partial P}{\partial z}$$
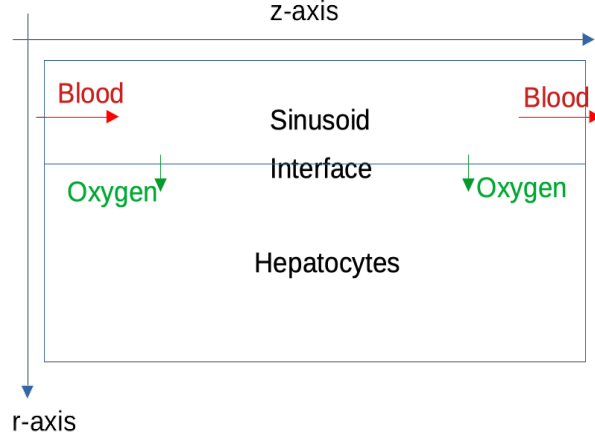
Figure 5 Schematic diagram of SysDILI domain setup and Oxygen Submodel. This setup is for the simulation of human liver sinusoid unit. 3D cylindrical coordinate system is centred at the top-left corner with z-axis horizontal. Blood with oxygen flows through the sinusoid, and some of the oxygen diffuses across the interface and gets consumed by hepatocytes.

- **Haemoglobin Oxygen**: convection equation was used, because oxygen does not diffuse when bound to haemoglobin.

$$\frac{\partial H}{\partial t} = -\boldsymbol{v} \cdot \nabla H = -v * \frac{\partial H}{\partial z}$$

- **Oxygen Equilibrium**: Hill equation was used to describe the haemoglobin-oxygen dissociation curve [27]. This only holds true when haemoglobin and plasma oxygen are in equilibrium (details in Section 2.1.1.2).

$$H = H_{max} * \frac{P^h}{P^h + K_A{}^h}$$

- **Oxygen in Hepatocytes**: diffusion-reaction was used, because there is no more convection of oxygen by blood flow. Michaelis-Menten kinetics was used for oxygen consumption by hepatocytes [24].

$$\frac{\partial O_2}{\partial t} = D_2 * \nabla^2 O_2 - R(O_2) = D_2 * \left(\frac{\partial^2 O_2}{\partial r^2} + \frac{\partial^2 O_2}{\partial z^2} + \frac{1}{r} * \frac{\partial O_2}{\partial r}\right) - \frac{O_2 * v_{max}}{O_2 + k_m}$$

- **Oxygen at the Interface**: equal-flux condition was used, because mass is conserved when oxygen moves across the interface [24].

$$D_1 * \frac{\partial P}{\partial r} = D_2 * \frac{\partial O_2}{\partial r}$$

P, H and O_2 are oxygen concentrations in hepatocyte, dissolved in plasma and bound to haemoglobin, respectively. D_1 and D_2 are oxygen diffusion coefficients in plasma and hepatocytes, respectively. v is sinusoid blood flow velocity assumed to be fixed in this model. v_{max} and k_m are constants for Michaelis-Menten kinetics of oxygen consumption in hepatocytes.

The PDE system was discretised both in time ($\Delta t = 4.5 * 10^{-3} s$) and space ($\Delta x = 2 \mu m$) before being simulated numerically. Details of the numerical algorithm, the boundary conditions and the choice of constants are elaborated in Methods section.

2.1.1.2 Haemoglobin Oxygen Release

Oxygen bound to haemoglobin is released when the plasma oxygen concentration decreases due to diffusion, moving down the haemoglobin-oxygen dissociation curve. The rate constant of oxyhemoglobin dissociation suggests that the process is much faster than oxygen diffusion in plasma [34]. Therefore, in the discretised numerical algorithm it was assumed that haemoglobin releases oxygen and the equilibrium is instantaneously reached at the end of each time step. This process is termed rebalancing, as shown in Figure 6, where P_n and $\bar{P}_n$ stand for plasma oxygen concentrations at n-th time step before and after rebalancing, respectively. Similarly, H_n and $\bar{H}_n$ represent concentrations of oxygen bound to haemoglobin at n-th time step before and after rebalancing, respectively.

$$
\begin{aligned}
\bar{P}_n + \bar{H}_n &= P_n + H_n \\
\bar{H}_n &= H_{max} * \frac{\bar{P}_n^h}{\bar{P}_n^h + K_A{}^h}
\end{aligned}
\tag{1}
$$

Equation 1 shows the exact procedure of rebalancing, during which $\bar{H}_n$ and $\bar{P}_n$ are solved from known H_n and P_n. Haemoglobin-oxygen dissociation curve is described by Hill equation, with the Hill coefficient h=2.73 and $K_A = 26$ mmHg, concentration of plasma oxygen with half of haemoglobin saturated [44]. $H_{max} = 6865.67$ mmHg is the total concentration of haemoglobin oxygen when haemoglobin is 100% saturated [44].
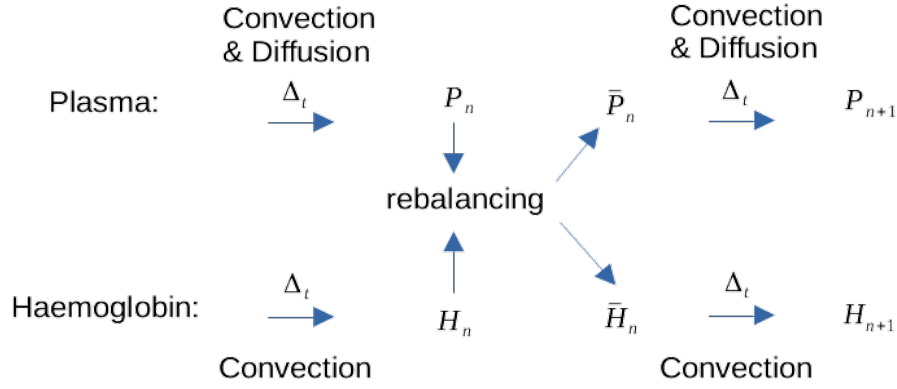
2.1.1.3 Validation

Figure 6 Schematic diagram of oxygen rebalancing in sinusoid. Haemoglobin oxygen and plasma oxygen are updated in parallel in each time step by different iteration matrices, but they get rebalanced to reach equilibrium at the end of time step, under the assumption that this process is relatively fast.

Figure 7 shows output of different domains from Oxygen Submodel. Gradients of oxygen concentration and oxygen consumption rate (OCR) were effectively created *in silico*. Figure 7a and Figure 7b show similar gradients because plasma oxygen and haemoglobin are in equilibrium, described by Hill equation. Figure 7c and Figure 7d show similar gradients because OCR versus oxygen concentration follows Michaelis-Menten kinetics and v_{max} is not reached. Both results were excepted and hence validate the simulation outcomes of Oxygen Submodel.

In human hepatic sinusoid, the plasma oxygen concentration is approximately 65 mmHg in zone 1 and 35 mmHg in zone 3 [20]. By fixing the boundary condition of plasma oxygen concentration at entry of zone 1 to be 65 mmHg, the simulated outcome at exit of zone 3 is close to 35 mmHg, as shown in Figure 8.

2.1.1.4 Sensitivity Analysis

Global sensitivity analysis of the average oxygen concentration in each zone to the parameters was carried out using Fourier amplitude sensitivity testing (FAST), and the results are shown in Figure 9. In all zones, oxygen concentration is the most sensitive to the change in v_{max}, the maximum OCR. Compared with other zones, oxygen concentration in zone 1 is more sensitive to oxygen input as expected, which validates the results.
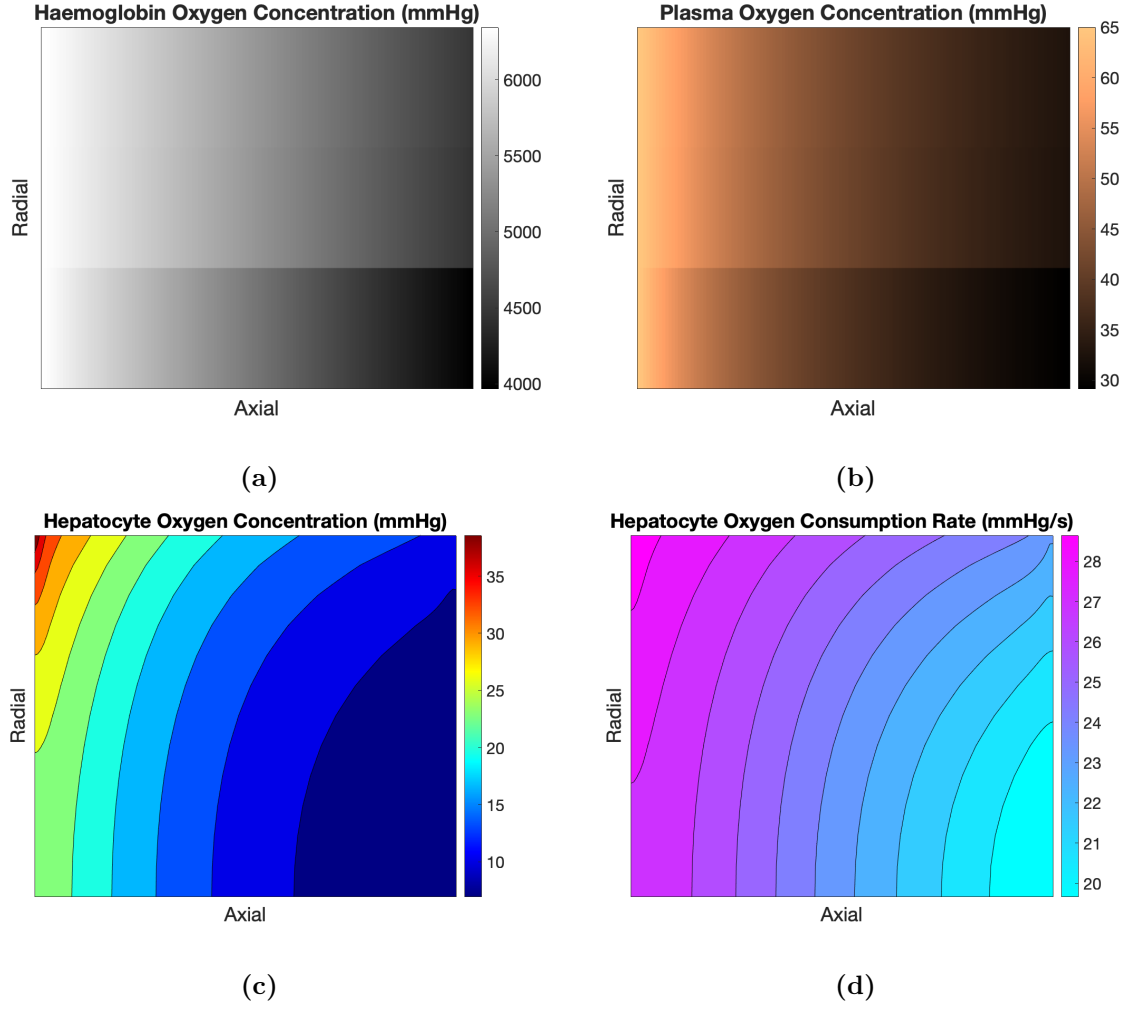
9

Figure 7 Simulation outcomes of Oxygen Submodel. (a) Haemoglobin oxygen concentration; (b) plasma oxygen concentration; (c) hepatocyte oxygen concentration; (d) hepatocyte oxygen consumption rate. The axes and layout in all plots are the same as those illustrated in Figure 5. Gradients of oxygen and oxygen consumption rate (OCR) were successfully simulated. (a) and (b), (c) and (d) have similar gradient patterns as expected.

The sensitivity analysis confirms the significance of Oxygen Submodel, because v_{max} will change from a parameter to a variable after Oxygen Submodel is assembled with Mitochondria or Density Submodel, while all other parameters are fixed to values from physiological data. When drug inhibits mitochondrial activities, maximum OCR of the cell will be reduced (see Section 2.1.2), resulting in significant change in oxygen concentration that would not have been taken into account if mitochondria was modelled alone [47].
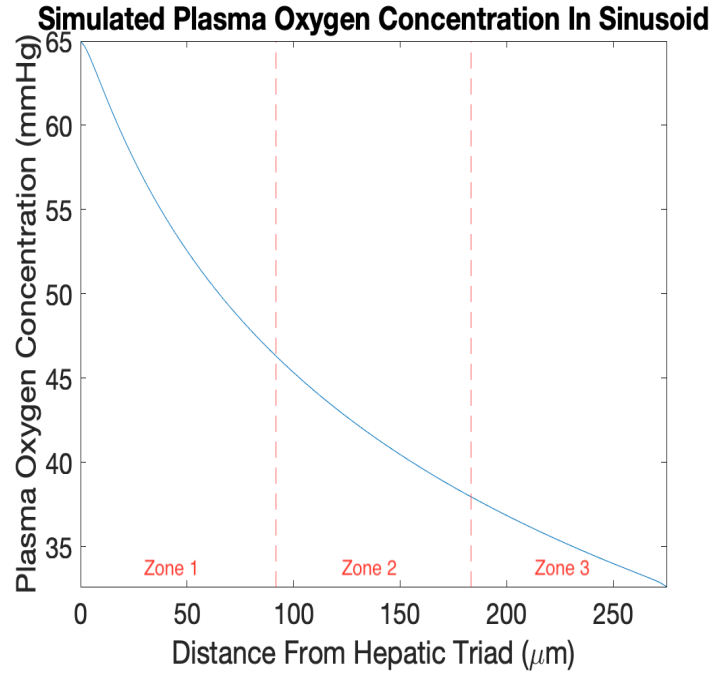
Figure 8 Simulated plasma oxygen concentration along the central axis of sinusoid. The oxygen input at the entrance of zone 1 was fixed to 65 mmHg as in the human liver, and then desired result of approximately 35 mmHg was observed in the simulation outcome of zone 3.

2.1.2 Mitochondria Submodel

The submodel was adapted and simplified from MITOsym$^{®}$ introduced in Yang et al., a mechanistic hepatocyte model of bioenergetics [47]. Three different toxicity mechanisms are supported: electron transport chain (ETC) inhibitor, uncoupler and ATPase inhibitor.
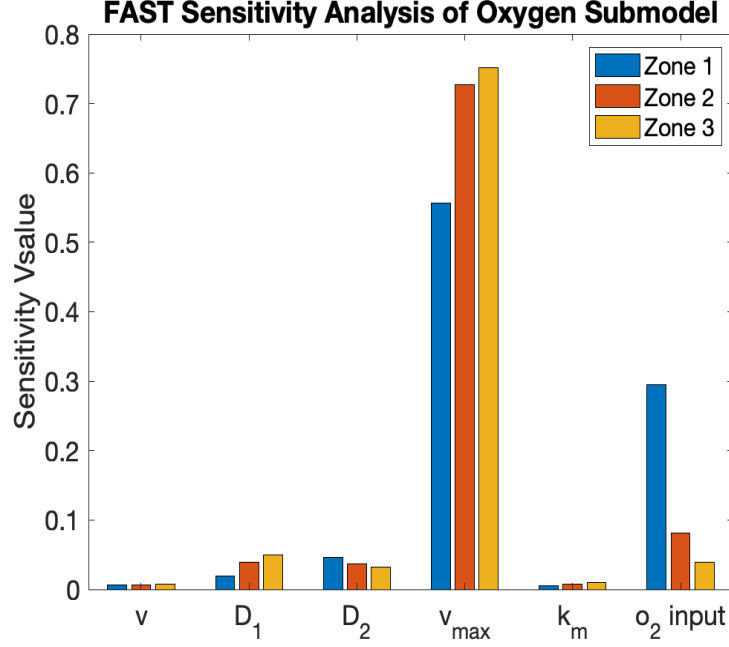
FAST Sensitivity Analysis of Oxygen Submodel

Figure 9 FAST Sensitivity analysis of average oxygen concentration in each zone to the parameters of Oxygen Submodel. O_2 input represents the Dirichlet boundary condition at the entrance of sinusoid. Range of each parameter was centred at the value picked for the model, with upper and lower bounds one order of magnitude apart. The results show that oxygen concentration is the most sensitive to v_{max}, especially in zone 3.

2.1.2.1 Model Structure

$$\frac{pyr2ox}{pyr2ox_{basal}} = \frac{k_1^{k_2} + \phi_{basal}^{k_2}}{k_1^{k_2} + \phi^{k_2}} * \frac{k_3^{k_4} + OX_{basal}^{k_4}}{k_3^{k_4} + OX^{k_4}}$$

$$\frac{dOX}{dt} = -ETCF + pyr2ox$$

$$OCR = q_1 * ETCF$$

$$ETCF = \frac{1}{q_1} * \frac{O_2 * v_{max}}{O_2 + k_m} * \frac{OX}{OX_{basal}} * drug_{etc} \qquad (2)$$

$$\frac{d\phi}{dt} = q_2 * ETCF - q_3 * ATPF - drug_{uncoupler}$$

$$ATPF = \frac{\phi * k_5}{\phi + q_4} * \frac{2 * ATPC_{basal}}{ATPC_{basal} + ATPC} * drug_{ATPase}$$

$$\frac{dATPC}{dt} = q_5 * ATPF - q_6 * ATPC$$

Variables	Meanings
pyr2ox	Rate of pyruvate as oxidative substrate in mitochondria
OX	Mitochondrial oxidative substrate
ETCF	Rate of oxidative substrate used for ETC activity, target of **ETC inhibitor**
OCR	Oxygen Consumption Rate
O_2	Oxygen concentration
ϕ	Mitochondrial Membrane Potential, target of **Uncoupler**
ATPF	Rate of mitochondria ATP production, target of **ATPase inhibitor**
ATPC	Cellular ATP

Table 1 Meanings of variables in Equation 2

$$drug_{etc} = \frac{km_1}{km_1 + C}$$
$$drug_{uncoupler} = \phi * \frac{k_6 * C}{km_2 + C} \qquad (3)$$
$$drug_{ATPase} = \frac{km_3}{km_3 + C}$$

Equation 2 defines the structure of the submodel, with the meanings of all variables listed in Table 1. Equation 3 defines the effect of drug with each toxicity mechanism, where C is the concentration of each drug respectively.

Figure 10 provides an schematic view of Equation 2. Figure 11 shows how the submodel relates to its predecessor, MITOsym®. The encircled variables and feedback signals remained in SysDILI. Three additional changes from MITOsym® are summarised below.

- Influx to pyr2ox, the first variable of the submodel, is constant.

- ETCF is affected by oxygen concentration, and their relation is described by Michaelis–Menten kinetics. This enables the interaction between Oxygen and Mitochondria Submodels.

- To calculate ATPC, ATPF is multiplied by a factor of $q_5 = \frac{4}{3}$ to compensate for glycolytic ATP that is not modelled (reasons and consequences in Discussion
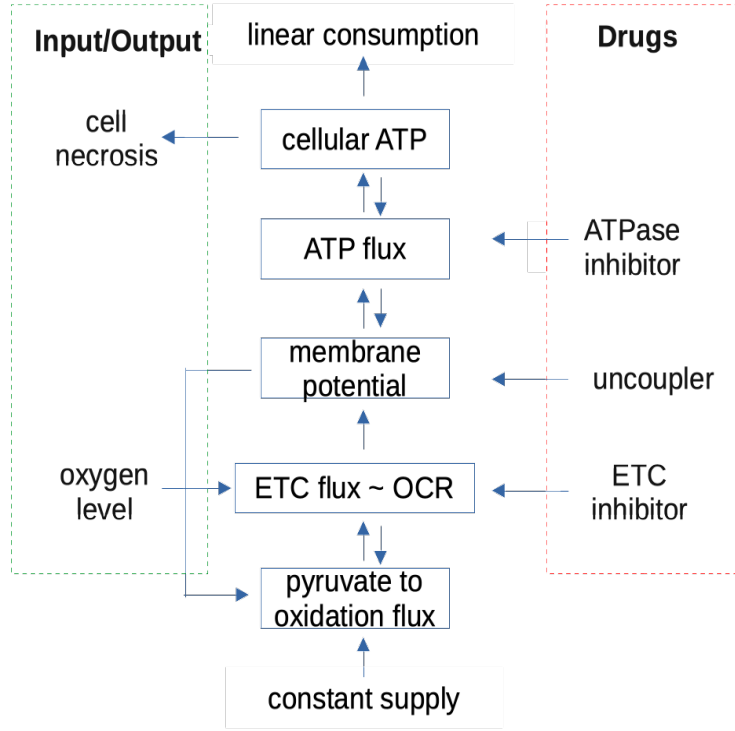
Figure 10 Schematic diagram of Mitochondria Submodel that illustrate Equation 2. Arrows going upwards represent the movement of fluxes in the metabolic pathway, while arrows going downwards represent feedback inhibitions. In the red box are the drugs with mitochondrial toxicity, and in the green box are the input and output of Mitochondria Submodel to other submodels of SysDILI.

section) .

2.1.2.2 Model Parametrisation

Figure 13a shows how the model parameters were determined during model construction. Basal values of all variables were given in Yang et al. $\{q_1, \dots, q_6\}$ and $\{k_1, \dots, k_6\}$ were estimated, because most of the parameter values were not provided by the authors. $\{q_1, \dots, q_6\}$ were determined in such a way that the basal values of variables were ensured to be an stationary point of the ODE system. Besides q_5 mentioned above, q_3 for $\frac{d\phi}{dt}$ was calculated using physiological data (see the Methods Section). $\{k_1, \dots, k_6\}$ were fitted using the batch of drug response data provided in Yang et al., nine data sets consisting of Rotenone (ETC inhibitor), FCCP (uncoupler) and Oligomycin (ATPase inhibitor) intakes versus OCR, ϕ, and ATPC.
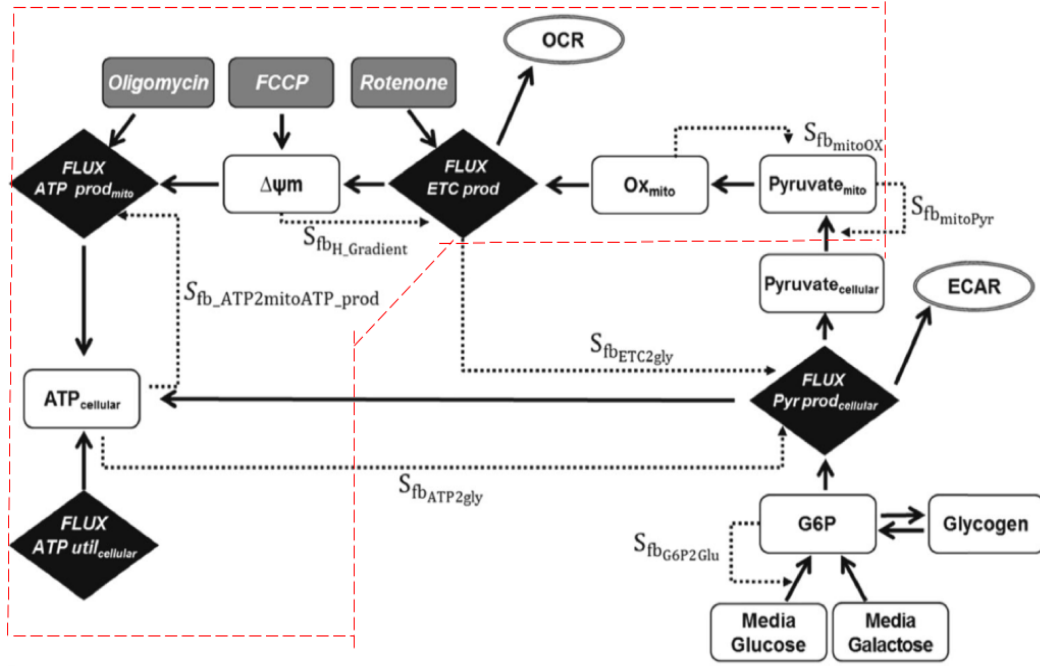
Figure 11 Schematic diagram of MITOsym® and its adaption. The encircled state variables, flux variables and feedback signals remained in SysDILI. Diagram adapted from Yang et al.[47]

Good fitting results of the model can be seen in Figure 12. The values of parameters are listed in Method Section.

2.1.2.3 Model Operation

Figure 13b shows how the model handles unknown drugs. All parameters determined during model construction stay constant. The mechanism and the dose-response curve of the unknown drug are needed as input, then the corresponding drug-specific km_i is fitted from dose-response curve, after which the simulation of this particular drug can be carried out. Alternatively, Michaelis constant (Km) can be supplied to reconstruct the dose-response curve of the unknown drug.

This procedure is different from that in Yang et al., where values of experimental Km were used directly for km_i in the model [47]. In contrast, the submodel treats km_i as nominal Km determined from experimental Km by optimisation, because the other variables might also changes with drug dose.
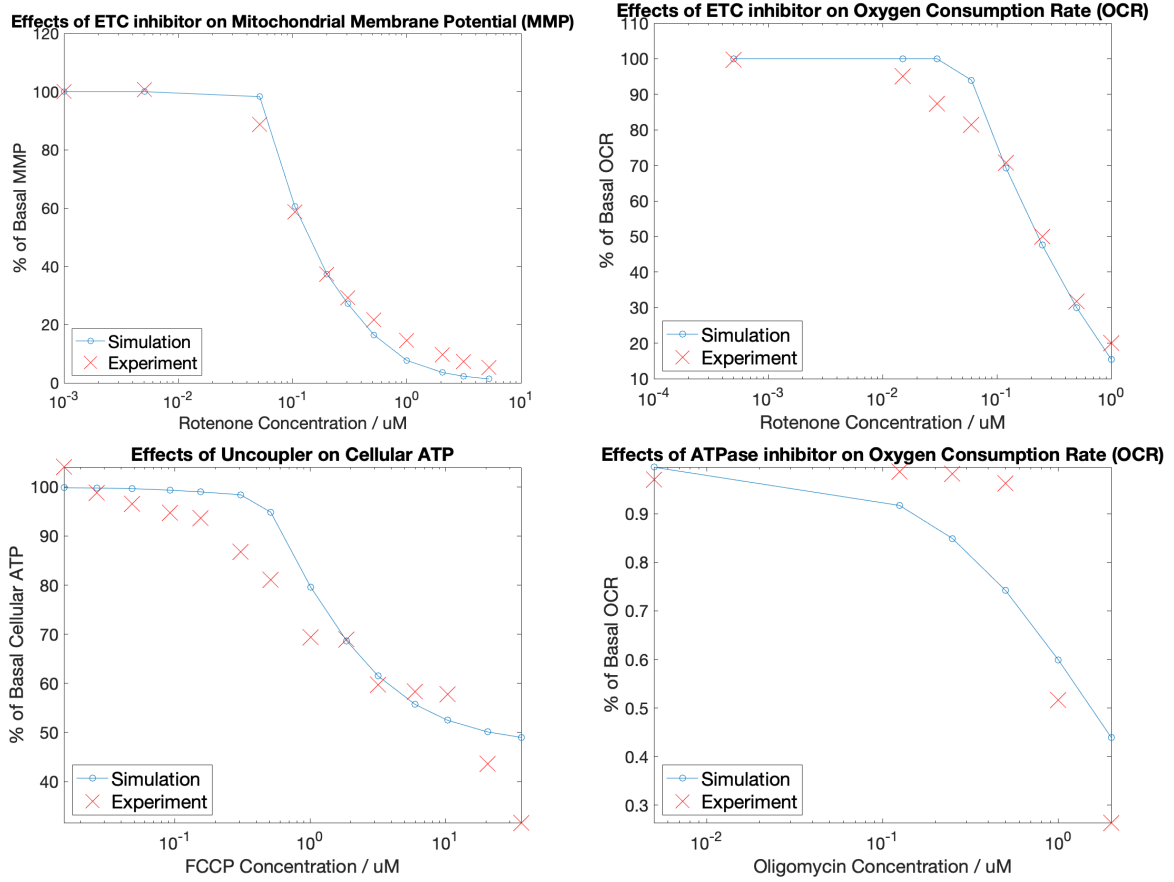
Figure 12 Goodness-of-fit for Mitochondria Submodel in selected datasets of dose-response. Clockwise from top-left: MMP versus Rotenone, OCR versus Rotenone, OCR versus Oligomycin, cellular ATP versus FCCP. Red crosses are experimental data, and the blue line are simulated results after fitting.

2.1.3 Cell Density Submodel

$$\frac{dDEN}{dt} = -(k_7 * \frac{AD^{k_9}}{AD^{k_9} + k_8{}^{k_9}} + k_{10} * \frac{AD^{k_{12}}}{AD^{k_{12}} + k_{11}{}^{k_{12}}}) * DEN \qquad (4)$$

Equation 4 defines Cell Density Submodel, where DEN is the density of hepatocytes and AD is the percentage decrease of cellular ATP. Note that AD=0 when cellular ATP is above the basal level.

This submodel was constructed from scratch. ATP depletion is the only input variable because it is regarded as an important cause of hepatocyte death [39]. Also, ATP depletion is relatively easy to track and linked directly to mitochondrial toxicity modelled in Mitochondria Submodel. Two Hill equation terms were used, motivated by
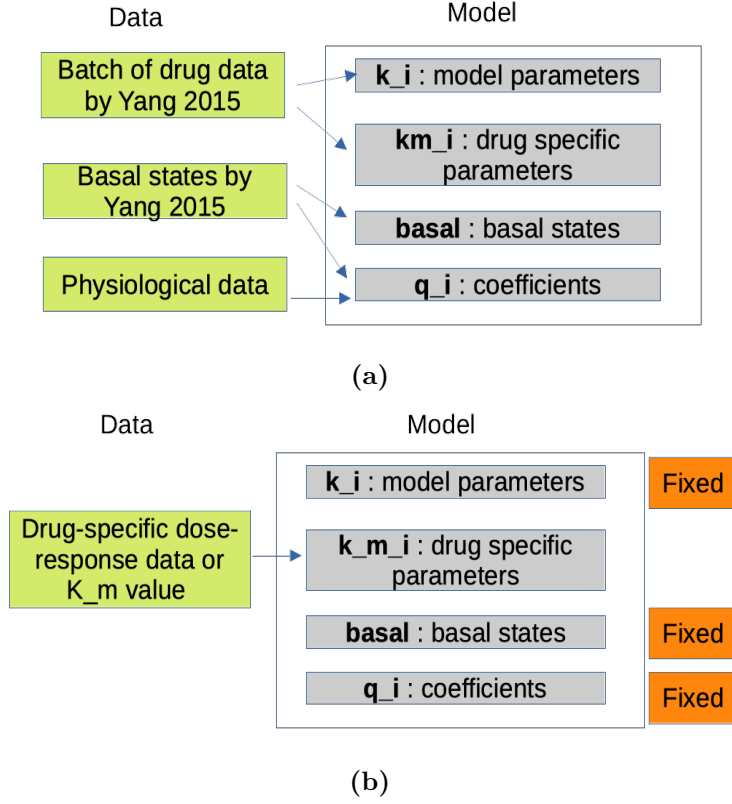
Figure 13 Schematic diagram of the parameters of Mitochondria Submodel. (a) Step One: determination of Mitochondria Submodel parameters during model construction; (b) Step Two: the operation of Mitochondria Submodel with an unknown drug, where all other parameters are fixed and the drug-specific parameters are fitted.

the finding that apoptosis and necrosis are both energy-dependent with ATP level as a switch between them [26, 43].

Only acute DILI (within 12 hours) was modelled in this submodel, because it is relatively easy to model and validate with existing data. Hepatocyte regeneration is negligible within this time range, so it is not modelled and the modelled cell density is monotonically decreasing in time [9]. Modelling longer term DILI might require a considerably more complex system.

2.1.3.1   Model Parametrisation

The parameters $\{k_7, \ldots, k_{12}\}$ were fitted using 10 datasets of cellular ATP versus time (input) and cell viability versus time (output) from Redegeld et al. [39, 38]. The exper-

iments were *in vitro* using rat hepatocytes, with lactate dehydrogenase (LDH) leakage as indicator for cell death, and only data from experiments with inhibition glycolytic ATP was selected (reasons in Discussion section).

Fitted results $k_7 = 80.5 \ min^{-1}$ and $k_{10} = 0.005 \ min^{-1}$ show that the two Hill equation terms in Equation 4 have completely different scales, an evidence that there exist two different energy-dependent processes for cell death, namely apoptosis and necrosis. Good fitting results can be seen in Figure 14.
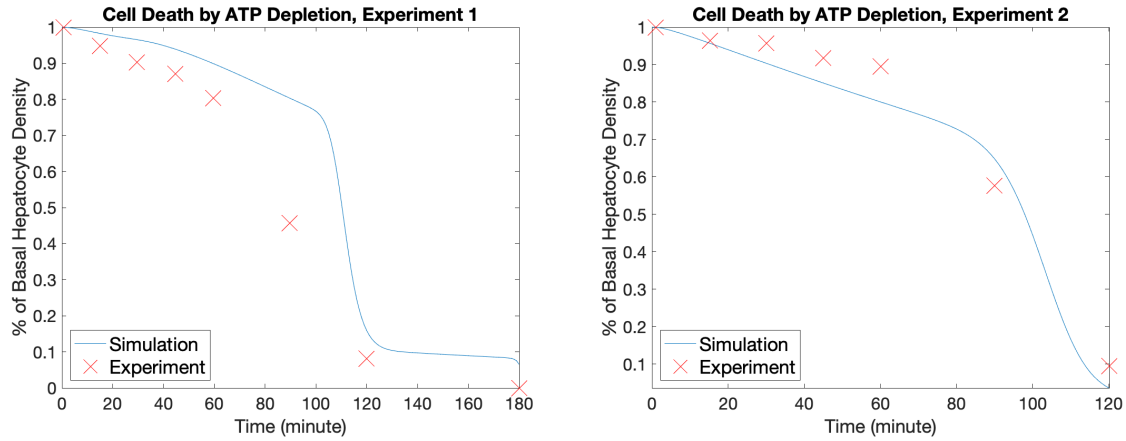

Figure 14 Goodness-of-fit for Cell Density Submodel in selected datasets of cell viability versus time. The corresponding input datasets of cellular ATP versus time are not shown. Red crosses represent experimental data, and the blue line represent simulated results after fitting.

2.1.4 Drug Submodel

Three options have been developed for Drug Submodel.

- **Option 1: Continuous Spatiotemporal Drug Gradient**: this setup is the same as Oxygen Submodel except an extra permeability coefficient when drug crosses cell membrane, modelled by changing the PDE at the sinusoid-hepatocyte interface to the following [25].

$$D_s * \frac{\partial C_s}{\partial r} = D_h * \frac{\partial C_h}{\partial r} = Q(C_s - C_h) \qquad (5)$$

  In Equation 5, Q is the drug-specific permeability coefficient. D_s and D_h are diffusion coefficients of drug in sinusoid and hepatocytes, respectively. C_s and
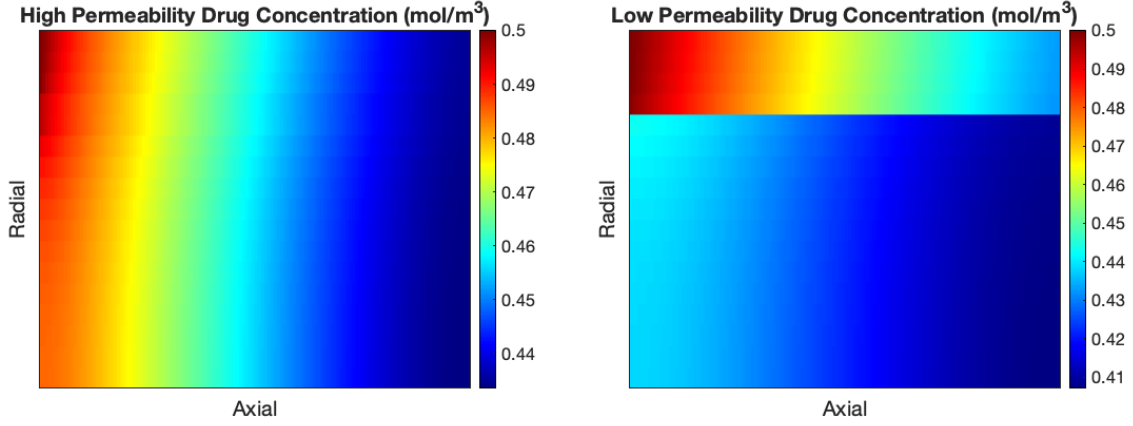
Figure 15 Output of Drug Submodel Option 1. The axes and layout are the same as those illustrated in Figure 5 of Oxygen Submodel. Q=4.8948 $\mu m/s$ and 0.0081 $\mu m/s$ were used to represent drugs with high and low permeability, respectively [25]. Drug gradients with different permeabilities were created as expected: high permeability leads to continuous gradient, while low permeability results in discontinuity at the interface.

C_h are the drug concentration in sinusoid and hepatocytes, respectively. In the numerical algorithm, this difference was modelled by increasing the interface from one unit to two to accommodate the extra condition $Q(C_s - C_h)$.

Figure 15 shows the output of drugs with high and low permeability. High permeability results in a radial gradient of drug concentration, while concentration discontinuity can be seen across the interface for drug with low permeability, as one would expected.

- **Option 2: Two-Compartment Model**: no drug gradient, only two compartments: sinusoid (central) and hepatocytes (peripheral). In Equation 6, k_{sh}, k_{hs}, k_e and $k_{metabolism}$ stand for first-order rate constants for drug distribution, redistribution, elimination and metabolism, respectively. I is the rate of drug input which may vary with time.

$$
\begin{aligned}
\frac{dC_s}{dt} &= -(k_e + k_{sh}) * C_s + k_{hs} * C_h + I \\
\frac{dC_h}{dt} &= -(k_m + k_{hs}) * C_h + k_{sh} * C_s
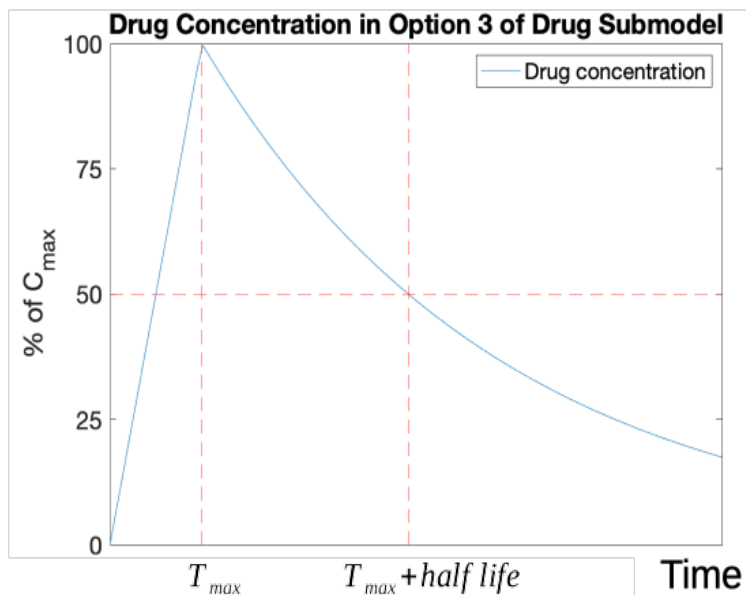\end{aligned}
\tag{6}
$$

19

Figure 16 Illustration of drug concentration over time in Option 3 of Drug Submodel. Drug concentration increases linearly and reaches C_{max} at time T_{max} before decreasing exponentially with fixed half life.

- **Option 3: One-Compartment Model**: hepatocytes domain is the only compartment. Drug concentration increases linear to reach C_{max} after time T_{max}, and then drops exponentially with a fixed half life, as illustrated in Figure 16.

Option 1 is more compatible with the theme of SysDILI, but it is difficult to validate in the context of human liver. Option 2 and 3 are pharmacokinetics model, so they might be more reliable and easier to parametrise with existing data. Option 3 was selected for the subsequent simulations, because human pharmacokinetics data of C_{max}, T_{max} and half life of drugs are readily available, which makes Option 3 easier to manipulate and track, allowing fair comparisons of different drugs. Option 1 and 2 might be used later in *in vitro* scenarios where measurement and manipulation are easier.

2.2 Toxicity Simulations

As said in Introduction section, submodels can be freely assembled for simulation. A few different combinations with increasing complexity have been tried. The mechanism of ETC inhibition was selected for simulations. Drugs and doses used in simulations are summarised in Table 2. Drug Submodel Option 3 was used with $T_{max} = 2$ hours

20

Trial IDs	Drug Names	k_m	Dose (C_{max})	Known Toxicity
A	Aripiprazole	0.75	0.1	0
B	Aripiprazole	0.75	0.2	0
C	Known Drug	2.7	1.3	0.5
D	Known Drug	2.7	5	1
E	Control	0.35	1.3	1
F	Control	0.35	5	1

Table 2 Drugs and doses in the simulations. Toxicity value of 0 means safe, 1 means toxic and 0.5 means moderately toxic.

and half life of 4.5 hours.
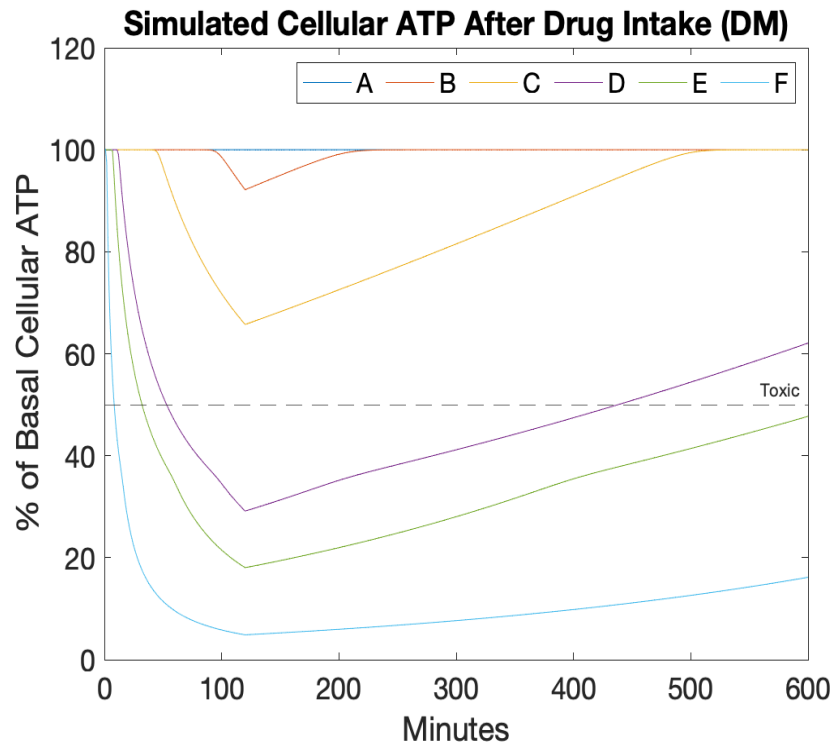
2.2.1   Drug+Mitochondria (DM)

Figure 17 Toxicity simulation outcome of DM model. Trial A and B shows very limited change in cellular ATP, implying safety. Cellular ATP of Trial D, E and F drop below toxicity criterion for a significant period, which agrees with their known toxicity. Trial C appears to be safe.

21

When Cell Density Submodel is not involved, cellular ATP level is used as surrogate. Cellular ATP lower than 50 percent of basal level implies toxicity, because it marks the onset of immune mediated induced necrosis by TNF-α [26, 33, 4]. No spatial gradient is involved in DM model, so oxygen concentration was fixed to the basal level in Mitochondria Submodel.

Figure 17 shows the outcome. Trial D, E and F were correctly predicted to be toxic, while Trial A and B were correctly predicted to be safe with almost no change to cellular ATP levels. However, Trial C was predicted to be safe, which is questionable. Further simulation and investigation are necessary.

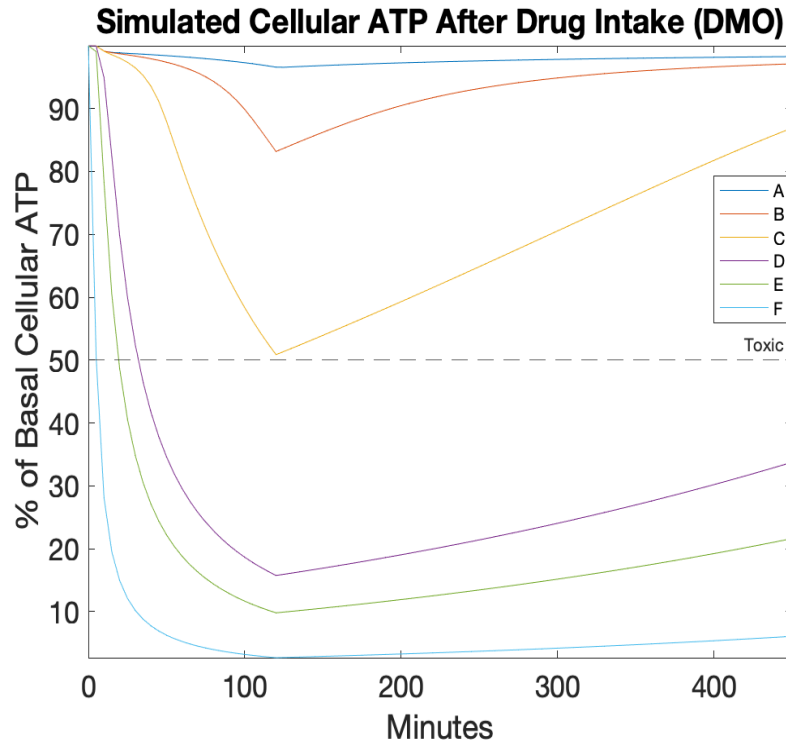### 2.2.2 Drug+Mitochondria+Oxygen (DMO)

Figure 18 Toxicity simulation outcome of DMO model. Cellular ATP level is the average of the entire hepatocytes domain. The outcome is similar to that of DM model in Figure 17, with result of Trial C correctly showing its mild toxicity.

Spatial gradients appeared after adding Oxygen Submodel. When assembling submodels, the spatially discretised domain setup of Oxygen Submodel was used, while

each discretised point received an independent copy of ODE-based Mitochondria Sub-model and Drug Submodel.

In the numerical simulation, equations of Oxygen and Mitochondria Submodels were not fused together into a larger PDE system, because the convergence of oxygen PDE system is much faster than the time step chosen for Mitochondria ODE system, 1 minute. Therefore, at the start of each time step, with OCR given by Mitochondria Submodel, Oxygen Submodel was run until convergence, producing an oxygen gradient for Mitochondria Submodel to use in the next time step.

Adding the oxygen gradient has rendered a more realistic result for Trial C, as shown in Figure 18.

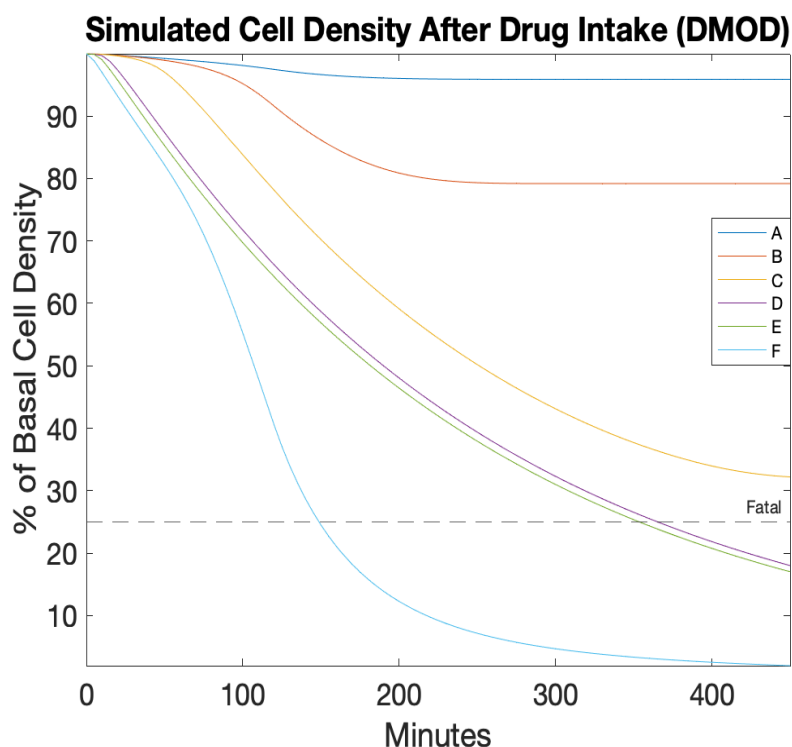### 2.2.3 Drug+Mitochondria+Oxygen+Density (DMOD)

Figure 19 Toxicity simulation outcome of DMOD model. Cell density level is the average of the entire hepatocytes domain. The toxicity predictions are similar to those in DMO model in Figure 18.
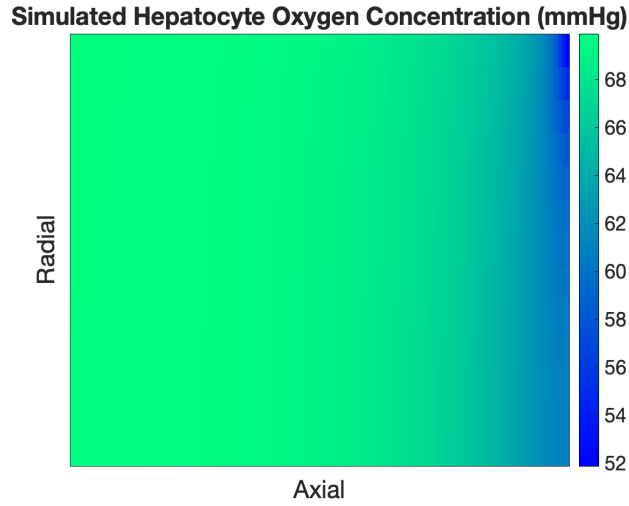
Figure 20 Hepatocyte Oxygen Concentration of Trial F in DMOD model after 450 minutes. Oxygen gradient is mostly lost when large dose of drug with mitochondrial toxicity causes severe DILI.

Figure 21 Cell Density of Trial D in DMOD model after 365 minutes. 25 percent marked with red dash line. Cell density is the lowest in zone 3, which indicates its relative vulnerability to DILI.

After adding Cell Density Submodel, cellular ATP is no longer needed as surrogate. Cell density below 25 percent of basal value is considered fatal damage [9].

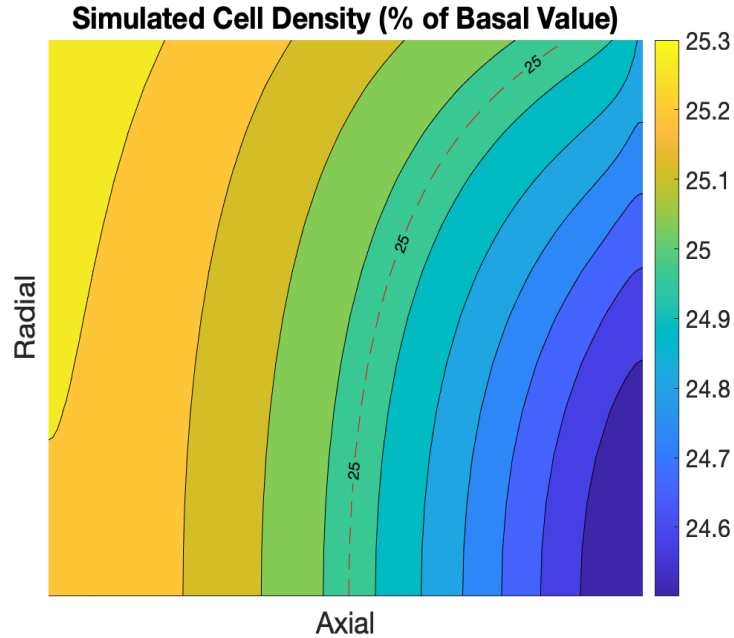Figure 19 shows the outcome of DMOD model. Trial D, E and F are confirmed to be fatally toxic, while Trial C is close to the borderline as expected. Apart from average values, simulated spatial gradients also contain useful insights. Research suggests that metabolic zonation of liver is often lost in liver diseases [22], as confirmed in Figure 20. When compared to Figure 7, simulated outcome of Trial F by DMOD model indicates that severe DILI damages the oxygen gradient. Figure 21 shows the simulated spatial distribution of cell density of Trial D, which indicates that zone 3 is relatively vulnerable to mitochondrial DILI, especially the part furthest away from hepatic sinusoid.

3 Discussion

The submodels of SysDILI have been developed independently. However, significant effort was made to ensure that the submodels work smoothly together and validate each other. Holistic approach of systems biology was used to study interactions quantitatively through PDEs and ODEs, allowing SysDILI to go beyond the reductionist approach of investigating each underlying process while fixing the others [42].

While some of the methods and models in SysDILI build on previous research, several new original advances have been incorporated in the presented analyses:

- Oxygen transport by haemoglobin was modelled dynamically, with the rebalancing process at the end of time step.

- km_i for the drugs in Mitochondrial Submodel were treated as nominal values and determined by optimisation, to handle the complexity of model.

- Two Hill equation terms were used in Cell Density Submodel to capture the combined effects of energy-dependent apoptosis and necrosis, instead of a separate model for each process. This "guided" black box model balances effectiveness and simplicity.

3.1 Model Design

SysDILI currently focuses on mitochondrial toxicity for two reasons. Firstly, mitochondria activities are relatively easy to measure and bioenergetics is well characterised. Secondly, mitochondria interacts well with other submodels. as shown in Figure 4, it is directly associated with respiration and oxygen gradient, as well as cell death by ATP depletion.

Instead of designating artificial zones or gradients, SysDILI was engineered to create the gradients by constructions to investigate the root cause. Liver zonation is an observed result of various gradients that regulate it. There is evidence that liver zonation is rather dynamic and not static, changing with the gradients [22]. Meanwhile, artificial gradients such as oxygen gradient was used to investigate its effects [21]. Acknowledging their effects, it is possible to go even deeper and uncover the cause of substance gradients, such as production, consumption and transport.

In Mitochondria Submodel, mitochondrial ATP was multiplied by a factor q_5 to account for glycolytic ATP. This might underestimate cellular ATP level when mitochondria activity gets inhibited, because glycolytic ATP production can alternatively be sustained by anaerobic glycolysis temporarily [16]. Another option is to fix glycolytic ATP at the basal value, but this instead overestimates cellular ATP, because sustained anaerobic analysis leads to the build-up of lactic acid, which eventually causes life-threatening lactic acidosis [16]. The treatment of glycolytic ATP that underestimates cellular ATP and hence drug safety was chosen, because it is conventional to have a conservative estimate for safety concern. Moreover, short term cell death in SysDILI might correspond to significant human DILI in longer term.

More importantly, hepatocyte viability is more sensitive to depletion of glycolytic ATP than mitochondrial ATP [39]. Redegeld et al. suggests that this might be due to the sub-cellular distribution of ATP: glycolytic ATP in the vicinity of cell membrane is more available to the ATP-driven processes at the membrane, which is the limiting factor in cell death [19]. For example, the calcium pump of cell membrane in pancreatic

cancer cell can be sustained by glycolytic ATP, and the cell survives without mitochondrial ATP [18]. Therefore, to parameterise Cell Density Model, only experiments with glycolysis inhibition were used, which again leads to underestimation of drug safety as expected.

3.2 Limitations and Potential Improvements

The focus of the project was on model construction and validation. Further research would be done to explore SysDILI and gain insight into drug-liver interactions, which was outside the scope of this research due to time restriction.

SysDILI relies on published data, which tend not to be ideal. The datasets used to parameterise each submodel are inconsistent. Parameters of HepaRG normal human hepatocyte were used in Oxygen Submodel, while all data used in Mitochondria Submodel is from HepG2 human liver cancer cell with lower metabolic activities than normal hepatocytes [45]. Cell Density Submodel were fitted with rat hepatocyte in *in vitro* setting. Therefore, despite each submodel being quantitative, at this stage SysDILI should be regarded as qualitative instead of quantitative model. The assumption is that the data inconsistency does not change the qualitative outcome.

Mitochondria Submodel can be upgraded to Bioenergetics Submodel by implementing the entire MITOsym and improving it ®. Variables of glycolytic ATP, lactate, glucose and glycogen will be available, after which toxicity mechanisms affecting glycolysis and glycogenolysis can be studied. Glycolytic ATP and mitochondrial ATP can be treated separately to eliminate the bias in Cell Density Submodel, the underestimation of drug safety mentioned above. Data from galactose-grown hepatocytes might be useful to isolate the effect of mitochondrial ATP, because galactose glycolysis yields no net ATP [5, 41]. A model of lactate might be introduced, because as an end product it might inhibit anaerobic glycolysis that sustains ATP production under mitochondrial dysfunction. It can potentially become a new stand-alone submodel of SysDILI, because liver is particularly important in lactate metabolism, accounting for 60 percent of lactate clearance through Cori cycle [28, 15] .

Mitochondria Submodel might also be used to infer the toxicity mechanism of an unknown drug. Given drug-response data of different variables, all km_i can be determined together through optimisation. The smaller km_i may indicate a bigger effect through that particular mechanism.

With lots of parameters in Mitochondria Submodel, a sensitivity analysis similar to that in Section 2.1.1.4 can benefit the understanding of the complicated interactions and identify the significant parameters for further investigation.

As mentioned before, Cell Density Submodel only models short term DILI within 12 hours for simplicity. It might be extended to model longer term DILI, with a more complex and mechanistic ODE system modelling mechanisms and regulatory pathways for regeneration, apoptosis and necrosis [9, 40]. Data from *in vitro* experiment of rat hepatocyte LDH might be replaced by *in vivo* measurement of Alanine transaminase (ALT), a commonly used indicator specific to human DILI [10, 46].

For Drug Submodel, more drugs with known T_{max} and half life can be simulated, instead of fixing these values. With more information of drug metabolic rates and mechanisms, Option 1 can be used to simulate MPS, where the intake of drug is easier to control than in *in vivo* scenarios.

The domain setup to model human liver can be improved by adding space of Disse. More molecules that are significant in liver zonation such as glucose and growth factors can be added, using models similar to Oxygen or Drug Submodel [22].

Domains and submodels can be easily changed or added to adapt to the setting of a particular MPS. Resources can be saved by narrowing down the range of drug dose for MPS experiments, using the toxicity predictions from SysDILI.

As for implementation, MATLAB codes might be made more organised using MAT-

Parameters	Values	Sources
Sinusoid Length	275 μm	Ehrlich et al. [6]
Sinusoid Diameter	10-15 μm (12.5 μm)	Maynard et al. [30]
Hepatocyte Diameter	25-30 μm (27.5 μm)	Meyer et al. [31]
v, Sinusoid Blood Flow Velocity	300-650 μm/s (400 μm/s)	Muller et al.[32]
v_{max} of hepatocyte OCR	44 μM/s	Leedale et al. [25]
k_m of hepatocyte OCR	6.24 μM	Leedale et al. [25]
O_2 Diffusion Coefficient in Plasma	2180 μm^2/s	Goldstick et al. [13]
O_2 Diffusion Coefficient in Hepatocytes	1600 μm^2/s	Leedale et al. [25]

Table 3 Human Physiological Parameters for Oxygen Submodel

LAB SimBiology toolbox, which takes care of variables and their units and streamlines model analysis. If large scale simulation is needed, the core program of SysDILI can be translated into Python.

4 Methods

All simulations, optimisations and visualisation were performed in MATLAB. The ODE systems for mitochondria, cell density and drug were solved numerically using ODE15s solver. The PDE systems (convection–diffusion-reaction equation) for oxygen and drug were solved by a numerical solver developed from scratch, using Crank-Nicolson method for diffusion, the upwind scheme for convection and Euler method for reaction. Parameters fitting for mitochondria and cell density were performed using multi-start global optimisation algorithm with interior-point method as the local optimiser available in MATLAB. For the rebalancing of haemoglobin and plasma oxygen, Equation 1 was solved by a Newton–Raphson method root finder developed from scratch to speed up simulations. Convergence was used as stopping criteria for the numerical simulations: $\frac{||M_{n+1}-M_n||}{\Delta t} < \epsilon$, where M_n is the matrix of variable at n-th time step. MATLAB Global Sensitivity Analysis Toolbox was used in FAST sensitivity analysis.

Table 3 lists parameters in Oxygen Submodel from human physiological data. Time

$(\Delta t = 4.5 * 10^{-3}s)$ and space $(\Delta x = 2\mu m)$ steps were chosen to satisfy the stability conditions of Crank-Nicolson method and the upwind scheme. Throughout Oxygen Submodel partial pressure with unit mmHg were used in place of concentration, because they are directly proportion by Henry's law with solubility coefficient of oxygen in plasma $\alpha = 3 \times 10^{-5}$ml O_2/ml plasma/mmHg [36].

For the boundary conditions of Oxygen Submodel (Figure 5), zero flux Neumann boundary condition was chosen for the boundary of hepatocytes domain. At the sinusoid entrance, plasma oxygen was given Dirichlet boundary condition as mentioned above while plasma and haemoglobin oxygen are in equilibrium. At the sinusiod exit, both plasma and haemoglobin oxygen have convection only, the diffusion of plasma oxygen at the exit is negligible.

$$
\begin{aligned}
\Delta\phi &= \frac{RT}{nF} * ln(\frac{[H^+]_{out}}{[H^+]_{in}}) \\
\frac{d\Delta\phi}{dt} &= \frac{RT}{nF} * (\frac{1}{[H^+]_{out}} * \frac{d[H^+]_{out}}{dt} - \frac{1}{[H^+]_{in}} * \frac{d[H^+]_{in}}{dt}) \\
&= \frac{RT}{nF} * (\frac{1}{[H^+]_{out}} + \frac{1}{[H^+]_{in}}) * \frac{dATP}{dt} * k_{[H+]/ATP} \\
&= \frac{RT}{nF} * (\frac{1}{10^{pH_{out}}} + \frac{1}{10^{pH_{in}}}) * \frac{dATP}{dt} * k_{[H+]/ATP} \\
\frac{d\Delta\phi}{dATP} &= \frac{RT}{nF} * (\frac{1}{10^{pH_{out}}} + \frac{1}{10^{pH_{in}}}) * k_{[H+]/ATP}
\end{aligned}
\tag{7}
$$

Table 4 lists the values of all parameters in Mitochondria and Cell Density Submodels. q_3, the change to MMP potential per unit of ATP produced, was calculated using physiological values. Nernst potential was differentiated to calculate this constant, as shown in Equation 7 [48]. $k_{[H+]/ATP} = 3$, because 3 protons are moved out to produce 1 ATP [3]. pH values of the mitochondrial matrix and the inter-membrane space are $pH_{in} = 7.78$ and $pH_{out} = 6.88$, respectively [37].

Parameters	Values	Methods	Sources
k_1	0.993 V	Optimisation	Yang et al. [47]
k_2	67	Optimisation	Yang et al. [47]
k_3	0.0372 mM	Optimisation	Yang et al. [47]
k_4	32.4	Optimisation	Yang et al. [47]
k_5	6787 mM min^{-1} V^{-1}	Optimisation	Yang et al. [47]
k_6	18971 min^{-1}	Optimisation	Yang et al. [47]
k_7	80.5 min^{-1}	Optimisation	Redegeld et al. [39, 38]
k_8	1.07	Optimisation	Redegeld et al. [39, 38]
k_9	88.6	Optimisation	Redegeld et al. [39, 38]
k_{10}	0.005 min^{-1}	Optimisation	Redegeld et al. [39, 38]
k_{11}	0.167	Optimisation	Redegeld et al. [39, 38]
k_{12}	0.877	Optimisation	Redegeld et al. [39, 38]
q_1	46 mmHg mM^{-1} min	Assumption/Basal	Yang et al. [47]
q_2	331 V mM^{-1}	Basal	Yang et al. [47]
q_3	0.199 V $pmol^{-1}$	Estimation/Calculation	see Methods Section
q_4	0.999 V	Basal	Yang et al. [47]
q_5	$\frac{4}{3}$	Assumption	see Results Section
q_6	3.70 mM^{-1}	Basal	Yang et al. [47]

Table 4 Parameters for Mitochondria Submodel and Cell Density Submodel. Methods of "Basal" means ensuring that basal values form a stationary point (see Results Section).

Acknowledgements

References

[1] DILIsym® - Drug-induced liver injury (DILI) modeling software. https://www.simulations-plus.com/software/dilisym/.

[2] Irene Anundi, Tuula Lähteenmäki, Mats Rundgren, Peter Moldeus, and Kai O. Lindros. Zonation of acetaminophen metabolism and cytochrome P450 2E1-mediated toxicity studied in isolated periportal and perivenous hepatocytes. *Biochemical Pharmacology*, 45(6):1251–1259, March 1993.

[3] M D Brand and A L Lehninger. H+/ATP ratio during ATP hydrolysis by mitochondria: Modification of the chemiosmotic theory. *Proceedings of the National Academy of Sciences of the United States of America*, 74(5):1955–1959, May 1977.

[4] John R. Cannon, Peter J. Harvison, and Glenn F. Rush. The effects of fructose on adenosine triphosphate depletion following mitochondrial dysfunction and lethal cell injury in isolated rat hepatocytes. *Toxicology and Applied Pharmacology*, 108(3):407–416, May 1991.

[5] J.A. Dykens and Y. Will. Mitochondrial Toxicity. In *Encyclopedia of Toxicology*, pages 349–353. Elsevier, 2014.

[6] Avner Ehrlich, Daniel Duche, Gladys Ouedraogo, and Yaakov Nahmias. Challenges and Opportunities in the Design of Liver-on-Chip Microdevices. *Annual Review of Biomedical Engineering*, 21:219–239, June 2019.

[7] Ye Fang and Richard M Eglen. Three-Dimensional Cell Cultures in Drug Discovery and Development. page 17.

[8] Toren Finkel. Signal Transduction by Mitochondrial Oxidants. *The Journal of Biological Chemistry*, 287(7):4434–4440, February 2012.

[9] Leon A. Furchtgott, Carson C. Chow, and Vipul Periwal. A Model of Liver Regeneration. *Biophysical Journal*, 96(10):3926–3935, May 2009.

[10] Edoardo G. Giannini, Roberto Testa, and Vincenzo Savarino. Liver enzyme alteration: A guide for clinicians. *CMAJ : Canadian Medical Association Journal*, 172(3):367–379, February 2005.

[11] Patricio Godoy, Nicola J. Hewitt, Ute Albrecht, Melvin E. Andersen, Nariman Ansari, Sudin Bhattacharya, Johannes Georg Bode, Jennifer Bolleyn, Christoph Borner, Jan Böttger, Albert Braeuning, Robert A. Budinsky, Britta Burkhardt, Neil R. Cameron, Giovanni Camussi, Chong-Su Cho, Yun-Jaie Choi, J. Craig Rowlands, Uta Dahmen, Georg Damm, Olaf Dirsch, María Teresa Donato, Jian Dong, Steven Dooley, Dirk Drasdo, Rowena Eakins, Karine Sá Ferreira, Valentina Fonsato, Joanna Fraczek, Rolf Gebhardt, Andrew Gibson, Matthias Glanemann, Chris E. P. Goldring, María José Gómez-Lechón, Geny M. M. Groothuis, Lena Gustavsson, Christelle Guyot, David Hallifax, Seddik Hammad, Adam Hayward, Dieter Häussinger, Claus Hellerbrand, Philip Hewitt, Stefan Hoehme, Hermann-Georg Holzhütter, J. Brian Houston, Jens Hrach, Kiyomi Ito, Hartmut Jaeschke, Verena Keitel, Jens M. Kelm, B. Kevin Park, Claus Kordes, Gerd A. Kullak-Ublick, Edward L. LeCluyse, Peng Lu, Jennifer Luebke-Wheeler, Anna Lutz, Daniel J. Maltman, Madlen Matz-Soja, Patrick McMullen, Irmgard Merfort, Simon Messner, Christoph Meyer, Jessica Mwinyi, Dean J. Naisbitt, Andreas K. Nussler, Peter Olinga, Francesco Pampaloni, Jingbo Pi, Linda Pluta, Stefan A. Przyborski, Anup Ramachandran, Vera Rogiers, Cliff Rowe, Celine Schelcher, Kathrin Schmich, Michael Schwarz, Bijay Singh, Ernst H. K. Stelzer, Bruno Stieger, Regina Stöber, Yuichi Sugiyama, Ciro Tetta, Wolfgang E. Thasler, Tamara Vanhaecke, Mathieu Vinken, Thomas S. Weiss, Agata Widera, Courtney G. Woods, Jinghai James Xu, Kathy M. Yarborough, and Jan G. Hengstler. Recent advances in 2D and 3D in vitro systems using primary hepatocytes, alternative hepatocyte sources and non-parenchymal liver cells and their use in investigating mechanisms of hepatotoxicity, cell signaling and ADME. *Archives of Toxicology*, 87(8):1315–1530, 2013.

[12] Daniel Goldman. Theoretical Models of Microvascular Oxygen Transport to Tissue. *Microcirculation (New York, N.Y. : 1994)*, 15(8):795–811, November 2008.

[13] T. K. Goldstick, V. T. Ciuryla, and L. Zuckerman. Diffusion of oxygen in plasma and blood. *Advances in Experimental Medicine and Biology*, 75:183–190, 1976.

[14] D M Grant. Detoxification Pathways in the Liver. page 2.

[15] Robert A. Harris. Energy Metabolism — Gluconeogenesis. In *Encyclopedia of Biological Chemistry III*, pages 170–186. Elsevier, 2021.

[16] Robert A. Harris and Justin S. Johnson. Energy Metabolism — Glycolysis Overview. In *Encyclopedia of Biological Chemistry III*, pages 141–148. Elsevier, 2019.

[17] Hartmut Jaeschke, Gregory J. Gores, Arthur I. Cederbaum, Jack A. Hinson, Dominique Pessayre, and John J. Lemasters. Mechanisms of Hepatotoxicity. *Toxicological Sciences*, 65(2):166–176, February 2002.

[18] Andrew D. James, Anthony Chan, Oihane Erice, Ajith K. Siriwardena, and Jason I.E. Bruce. Glycolytic ATP Fuels the Plasma Membrane Calcium Pump Critical for Pancreatic Cancer Cell Survival. *Journal of Biological Chemistry*, 288(50):36007–36019, December 2013.

[19] D. P. Jones. Intracellular diffusion gradients of O2 and ATP. *American Journal of Physiology-Cell Physiology*, 250(5):C663–C675, May 1986.

[20] Kurt Jungermann and Thomas Kietzmann. Oxygen: Modulator of metabolic zonation and disease of the liver. *Hepatology*, 31(2):255–260, 2000.

[21] Young Bok Kang, Jinsu Eo, Safak Mert, Martin L. Yarmush, and O. Berk Usta. Metabolic Patterning on a Chip: Towards in vitro Liver Zonation of Primary Rat and Human Hepatocytes. *Scientific Reports*, 8(1):8951, December 2018.

[22] Thomas Kietzmann. Metabolic zonation of the liver: The oxygen gradient revisited. *Redox Biology*, 11:622–630, April 2017.

[23] Felipe T Lee-Montiel, Subin M George, Albert H Gough, Anup D Sharma, Juanfang Wu, Richard DeBiasio, Lawrence A Vernetti, and D Lansing Taylor. Control

of oxygen tension recapitulates zone-specific functions in human liver microphysiology systems. *Experimental Biology and Medicine*, 242(16):1617–1632, October 2017.

[24] Joseph Leedale, Helen E. Colley, Harriet Gaskell, Dominic P. Williams, Rachel N. Bearon, Amy E. Chadwick, Craig Murdoch, and Steven D. Webb. In silico-guided optimisation of oxygen gradients in hepatic spheroids. *Computational Toxicology*, 12:100093, November 2019.

[25] Joseph A. Leedale, Jonathan A. Kyffin, Amy L. Harding, Helen E. Colley, Craig Murdoch, Parveen Sharma, Dominic P. Williams, Steven D. Webb, and Rachel N. Bearon. Multiscale modelling of drug transport and metabolism in liver spheroids. *Interface Focus*, 10(2):20190041, April 2020.

[26] Marcel Leist, Barbara Single, Anna F. Castoldi, Simone Kühnle, and Pierluigi Nicotera. Intracellular Adenosine Triphosphate (ATP) Concentration: A Switch in the Decision Between Apoptosis and Necrosis. *Journal of Experimental Medicine*, 185(8):1481–1486, April 1997.

[27] Melvin Khee-Shing Leow. Configuration of the hemoglobin oxygen dissociation curve demystified: A basic mathematical proof for medical and biological sciences undergraduates. *Advances in Physiology Education*, 31(2):198–201, June 2007.

[28] Bruno Levy. Lactate and shock state: The metabolic view. *Current Opinion in Critical Care*, 12(4):315–321, August 2006.

[29] Rita Manco and Shalev Itzkovitz. Liver zonation. *Journal of Hepatology*, 74(2):466–468, February 2021.

[30] Robert Lewis Maynard and Noel Downes. Chapter 14 - Liver. In Robert Lewis Maynard and Noel Downes, editors, *Anatomy and Histology of the Laboratory Rat in Toxicology and Biomedical Research*, pages 159–168. Academic Press, January 2019.

[31] Denny J. Meyer. Chapter 9 - The Liver. In Rose E. Raskin and Denny J. Meyer, editors, *Canine and Feline Cytology (Third Edition)*, pages 259–283. W.B. Saunders, St. Louis, January 2016.

[32] Michael Müller, René Keimling, Sascha Lang, Josef Pauli, Uta Dahmen, and Olaf Dirsch. Estimating Blood Flow Velocity in Liver Vessels. In W. Brauer, Hans-Peter Meinzer, Thomas Martin Deserno, Heinz Handels, and Thomas Tolxdorff, editors, *Bildverarbeitung Für Die Medizin 2009*, pages 36–40. Springer Berlin Heidelberg, Berlin, Heidelberg, 2009.

[33] A. L. Nieminen, A. K. Saylor, B. Herman, and J. J. Lemasters. ATP depletion rather than mitochondrial depolarization mediates hepatocyte killing after metabolic inhibition. *American Journal of Physiology-Cell Physiology*, 267(1):C67–C74, July 1994.

[34] John S. Olson, Erin W. Foley, David H. Maillett, and Eden V. Paster. *Measurement of Rate Constants for Reactions of O_2, CO, and NO with Hemoglobin*, volume 82, pages 065–091. Humana Press, New Jersey, March 2003.

[35] Samantha Peel, Adam M. Corrigan, Beate Ehrhardt, Kyung-Jin Jang, Pedro Caetano-Pinto, Matthew Boeckeler, Jonathan E. Rubins, Konstantia Kodella, Debora B. Petropolis, Janey Ronxhi, Gauri Kulkarni, Alison J. Foster, Dominic Williams, Geraldine A. Hamilton, and Lorna Ewart. Introducing an automated high content confocal imaging approach for Organs-on-Chips. *Lab on a Chip*, 19(3):410–421, 2019.

[36] Roland N. Pittman. *Oxygen Transport*. Morgan & Claypool Life Sciences, 2011.

[37] Anna Maria Porcelli, Anna Ghelli, Claudia Zanna, Paolo Pinton, Rosario Rizzuto, and Michela Rugolo. pH difference across the outer mitochondrial membrane measured with a green fluorescent protein mutant. *Biochemical and Biophysical Research Communications*, 326(4):799–804, January 2005.

[38] Frank A. M. Redegeld, Ralf M. W. Moison, Helma M. Barentsen, Andries Sj. Koster, and Jan Noordhoek. Interaction with cellular ATP generating pathways

mediates menadione-induced cytotoxicity in isolated rat hepatocytes. *Archives of Biochemistry and Biophysics*, 280(1):130–136, July 1990.

[39] Frank A.M. Redegeld, Ralf M.W. Moison, Andries S. Koster, and Jan Noordhoek. Depletion of ATP but not of GSH affects viability of rat hepatocytes. *European Journal of Pharmacology: Environmental Toxicology and Pharmacology*, 228(4):229–236, December 1992.

[40] Christopher H. Remien, Frederick R. Adler, Lindsey Waddoups, Terry D. Box, and Norman L. Sussman. Mathematical modeling of liver injury and dysfunction after acetaminophen overdose: Early discrimination between survival and death. *Hepatology*, 56(2):727–734, August 2012.

[41] Reika Shiratori, Kenta Furuichi, Masashi Yamaguchi, Natsumi Miyazaki, Haruna Aoki, Hiroji Chibana, Kousei Ito, and Shigeki Aoki. Glycolytic suppression dramatically changes the intracellular metabolic profile of multiple cancer cell lines in a mitochondrial metabolism-dependent manner. *Scientific Reports*, 9(1):18699, December 2019.

[42] Iman Tavassoly, Joseph Goldfarb, and Ravi Iyengar. Systems biology primer: The basic methods and approaches. *Essays in Biochemistry*, 62(4):487–500, October 2018.

[43] Yoshihide Tsujimoto. Apoptosis and necrosis: Intracellular ATP level as a determinant for cell death modes. *Cell Death & Differentiation*, 4(6):429–434, August 1997.

[44] Romain Valabrègue, Agnès Aubert, Jacques Burger, Jacques Bittoun, and Robert Costalat. Relation between Cerebral Blood Flow and Metabolism Explained by a Model of Oxygen Exchange. *Journal of Cerebral Blood Flow & Metabolism*, 23(5):536–545, May 2003.

[45] Mathieu Vinken and Vera Rogiers, editors. *Protocols in in Vitro Hepatocyte Research*. Number 1250 in Methods in Molecular Biology. Humana Press, New York, 2015.

[46] P B Watkins. Drug Safety Sciences and the Bottleneck in Drug Development. *Clinical Pharmacology & Therapeutics*, 89(6):788–790, June 2011.

[47] Y. Yang, S. Nadanaciva, Y. Will, J. L. Woodhead, B. A. Howell, P. B. Watkins, and S. Q. Siler. MITOsym®: A Mechanistic, Mathematical Model of Hepatocellular Respiration and Bioenergetics. *Pharmaceutical Research*, 32(6):1975–1992, June 2015.

[48] Ljubava D. Zorova, Vasily A. Popkov, Egor Y. Plotnikov, Denis N. Silachev, Irina B. Pevzner, Stanislovas S. Jankauskas, Valentina A. Babenko, Savva D. Zorov, Anastasia V. Balakireva, Magdalena Juhaszova, Steven J. Sollott, and Dmitry B. Zorov. Mitochondrial membrane potential. *Analytical biochemistry*, 552:50–59, July 2018.